Chapter 6

In Pursuit of Angular Trispectrum

The angular trispectrum, the harmonic transform of the angular four-point correlation function, carries cosmological information which is independent of the power spectrum and the bispectrum.

Several authors show that the weak lensing effect produces non-trivial connected CMB angular trispectrum or four-point correlation function on small angular scales (Bernardeau, 1997; Zaldarriaga and Seljak, 1999; Zaldarriaga, 2000; Hu, 2001). On large angular scales, Inoue (2001a,b) shows that the connected trispectrum is produced if topology of our universe is closed flat or closed hyperbolic. These effects do not produce the bispectrum, the angular three-point harmonic spectrum, but the trispectrum. Hence, while we have not found significant bispectrum on the DMR map in chapter 5, we could find the trispectrum.

The connected angular trispectrum contributes to the power spectrum covariance matrix. It increases the variance, and produces non-zero off-diagonal terms in the covariance matrix. Measuring the connected trispectrum thus constrains how much the connected trispectrum contributes to the power spectrum covariance. This is important to do. We have to know the power spectrum covariance matrix as accurate as possible, when we measure the power spectrum with better than 1% accuracy, and determine many of cosmological parameters with better than 10% accuracy.

So far, there has been no attempt to measure the angular trispectrum of the CMB anisotropy. In this chapter, we present the first measurement of the CMB trispectrum on the DMR map. We measure all independent terms of the angular trispectrum down to the DMR beam size, and test Gaussianity of the DMR data.

This chapter is organized as follows. In § 6.1, we give our method of measuring the angular trispectrum from CMB sky maps. In § 6.2, we study statistical properties of the normalized trispectrum. In § 6.3, applying the method to the DMR data, we measure the angular trispectrum. We then test Gaussianity of the DMR data with the normalized trispectrum. Finally, § 6.4 concludes this chapter,

6.1 Angular Trispectrum

The angular trispectrum comprises four harmonic transforms of the CMB temperature anisotropy field, $a_{l_1m_1}a_{l_2m_2}a_{l_3m_3}a_{l_4m_4}$, where

$$a_{lm} = \int_{\Omega_{\rm obs}} d^2\hat{\mathbf{n}}\, \frac{\Delta T(\hat{\mathbf{n}})}{T} Y^*_{lm}(\hat{\mathbf{n}}). \tag{6.1}$$

$\Omega_{\rm obs}$ denotes a solid angle of the observed sky. A rotationally invariant angular averaged trispectrum, $T^{l_1l_2}_{l_3l_4}(L)$, takes the form (Hu, 2001)

$$\begin{aligned} T^{l_1l_2}_{l_3l_4}(L) &= (2L+1)\sum_{\text{all } m}\sum_{M}(-1)^M \begin{pmatrix} l_1 & l_2 & L \\ m_1 & m_2 & M \end{pmatrix}\begin{pmatrix} l_3 & l_4 & L \\ m_3 & m_4 & -M \end{pmatrix} \\ &\quad \times a_{l_1m_1}a_{l_2m_2}a_{l_3m_3}a_{l_4m_4}, \end{aligned} \tag{6.2}$$

where the Matrices denote the Wigner-$3j$ symbol. By construction, l_1, l_2, and L form one triangle, while l_3, l_4, and L form the other triangle in a quadrilateral with sides of l_1, l_2, l_3, and l_4. L represents a diagonal of the quadrilateral. Figure 3.5 sketches a configuration of the angular trispectrum. When we arrange l_1, l_2, l_3, and l_4 in order of $l_1 \le l_2 \le l_3 \le l_4$, L lies in $\max(l_2 - l_1, l_4 - l_3) \le L \le \min(l_1 + l_2, l_3 + l_4)$. Hence, $l_1 = l_2$ and $l_3 = l_4$ for $L = 0$. Parity invariance of the angular four-point correlation function demands $l_1+l_2+L = $ even and $l_3+l_4+L = $ even.

The angular trispectrum generically consists of two parts. One part is the unconnected part, the contribution from Gaussian fields, which is given by the angular power spectra (Hu, 2001),

$$\begin{aligned} \left\langle T^{l_1l_2}_{l_3l_4}(L)\right\rangle_{\rm unconnected} &= (-1)^{l_1+l_3}\sqrt{(2l_1+1)(2l_3+1)}\,\langle C_{l_1}\rangle\langle C_{l_3}\rangle\,\delta_{l_1l_2}\delta_{l_3l_4}\delta_{L0} \\ &\quad +(2L+1)\langle C_{l_1}\rangle\langle C_{l_2}\rangle\left[(-1)^{l_2+l_3+L}\delta_{l_1l_3}\delta_{l_2l_4} + \delta_{l_1l_4}\delta_{l_2l_3}\right]. \end{aligned} \tag{6.3}$$

For $l_1 \le l_2 \le l_3 \le l_4$, the unconnected terms are non-zero only when $L = 0$ or $l_1 = l_2 = l_3 = l_4$. We have numerically confirmed that our estimator given below (Eq.(6.4)) accurately reproduces the unconnected terms (Eq.(6.3)) on a simulated Gaussian sky.

The other part is the connected part whose expectation value is exactly zero for Gaussian fields; thus, the connected part is sensitive to non-Gaussianity. When none of l's are same in $T^{l_1l_2}_{l_3l_4}(L)$, one might expect the trispectrum to comprise the connected part only; however, it is true only on the full sky. The unconnected terms on the incomplete sky, which are often much bigger than the connected terms, leak the power to the other modes for which all l's are different. We should take this effect into account in the analysis.

Using the azimuthally averaged harmonic transform, $e_l(\hat{\mathbf{n}})$ (Eq.(3.9)), we rewrite equation (6.2) into a much more computationally efficient form,

$$T^{l_1l_2}_{l_3l_4}(L) = \frac{1}{2L+1}\sum_{M=-L}^{L} t^{l_1l_2*}_{LM}\, t^{l_3l_4}_{LM}, \tag{6.4}$$

where

$$t^{l_1l_2}_{LM} \equiv \sqrt{\frac{2L+1}{4\pi}}\begin{pmatrix} l_1 & l_2 & L \\ 0 & 0 & 0 \end{pmatrix}^{-1}\int d^2\hat{\mathbf{n}}\,\left[e_{l_1}(\hat{\mathbf{n}})e_{l_2}(\hat{\mathbf{n}})\right]Y^*_{LM}(\hat{\mathbf{n}}). \tag{6.5}$$

Since $t^{l_1 l_2}_{LM}$ is the harmonic transform on the full sky, we can calculate it quickly. This method makes measurement of the angular trispectrum computationally feasible even for the *MAP* data in which we have more than millions of pixels; thus, the methods developed here can be applied not only to the *COBE* DMR data, but also to the *MAP* data.

For the DMR data for which the maximum l_4 is 20, we have 21,012 non-zero trispectrum modes after taking into account the triangle conditions in a quadrilateral and parity invariance. Measurement of 21,012 modes takes about 5 second of CPU time on a Pentium-III single processor personal computer.

We use Monte-Carlo simulations to estimate the covariance matrix of the angular trispectrum. We have described details of our simulations in chapter 5. We generate 5,000 realizations for one simulation; processing one realization takes about 5 second, so that one simulation takes about 7 hours of CPU time on a Pentium-III single processor personal computer. In total, we run 6 simulations, generating 30,000 realizations.

6.2 Normalized Trispectrum

In general, analytic forms of the angular trispectrum covariance, $\left\langle T^{l_1 l_2}_{l_3 l_4}(L) T^{l'_1 l'_2}_{l'_3 l'_4}(L') \right\rangle$, are highly complicated (Hu, 2000); however, one can reduce them to rather simplified forms for $l_1 \le l_2 < l_3 \le l_4$ and $L \neq 0$ (chapter 3). The covariance of these terms on the full sky is diagonal, and the variance is given by equation (3.34),

$$\left\langle \left[T^{l_1 l_2}_{l_3 l_4}(L) \right]^2 \right\rangle = (2L+1) \langle C_{l_1} \rangle \langle C_{l_2} \rangle \langle C_{l_3} \rangle \langle C_{l_4} \rangle \left(1 + \delta_{l_1 l_2} + \delta_{l_3 l_4} + \delta_{l_1 l_2} \delta_{l_3 l_4}\right). \tag{6.6}$$

One finds that the variance of the trispectrum is very sensitive to the power spectrum normalization. A slight difference in the power spectrum normalization alters the variance of the trispectrum substantially. This makes a test for Gaussianity with the "bare" trispectrum very difficult, as it requires precise determination of the power spectrum normalization.

We overcome the difficulty by normalizing the trispectrum as

$$\frac{T^{l_1 l_2}_{l_3 l_4}(L)}{\left[(2L+1) C_{l_1} C_{l_2} C_{l_3} C_{l_4}\right]^{1/2}}. \tag{6.7}$$

This statistic, the normalized trispectrum, is analogous to the normalized bispectrum that we have used in chapter 5. As similar to the normalized bispectrum, the variance of the normalized trispectrum is insensitive to the power spectrum normalization, and systematically smaller than that of the bare trispectrum. The normalized trispectrum is thus reasonably sensitive to non-Gaussianity.

Figure 6.1 compares the variance of the normalized trispectrum with that of the bare trispectrum, for full sky coverage as well as for incomplete sky coverage. We have used $l_1 \le l_2 < l_3 \le l_4$ and $L \neq 0$ terms, and calculated the variance from simulated realizations of a Gaussian sky. We confirm that the variance of the normalized trispectrum is systematically smaller than that of the bare trispectrum, and that the variance distribution becomes more scattered on the incomplete sky.

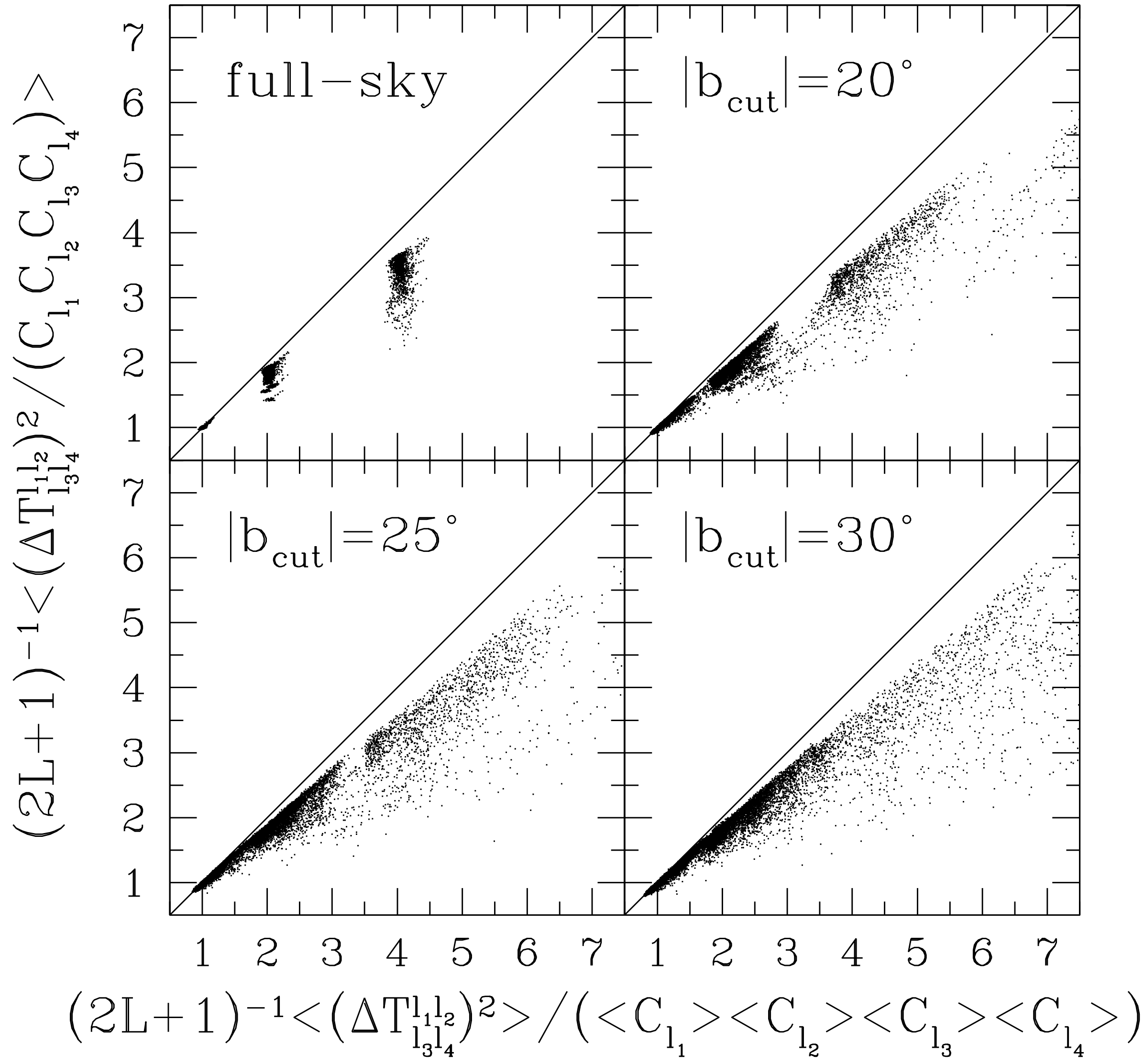

Figure 6.1: Variance of Normalized Trispectrum and Bare Trispectrum

Comparison of the variance of the normalized trispectrum with that of the bare trispectrum for $l_1 \leq l_2 < l_3 \leq l_4$ and $L \neq 0$ (group (a)). These are derived from simulated realizations of a Gaussian sky. The top-left panel shows the case of full sky coverage, while the rest of panels show the cases of incomplete sky coverage. The top-right, bottom-left, and bottom-right panels use the 20°, 25°, and 30° Galactic cuts, respectively.

6.3 Testing Gaussianity of the DMR Map

In this section, we test Gaussianity of the DMR data using the normalized trispectrum. Before performing the analysis, we should recall that even if CMB is exactly Gaussian, there are significant, non-zero unconnected trispectrum terms for $L = 0$ or $l_1 = l_2 = l_3 = l_4$. We should analyze these configurations separately from the others for which the unconnected terms vanish.

6.3.1 Classification of trispectrum configurations

We divide the measured 21,012 modes into four groups:

(a) $l_2 \neq l_3$, and $L \neq 0$ (16,554 modes)

(b) $l_2 = l_3$, $l_1 \neq l_4$, and $L \neq 0$ (4,059 modes)

(c) $l_1 = l_2 = l_3 = l_4$, and $L \neq 0$ (209 modes)

(d) $L = 0$ (190 modes)

Note that all the groups satisfy $l_1 \leq l_2 \leq l_3 \leq l_4$, $\max(l_2 - l_1, l_4 - l_3) \leq L \leq \min(l_1 + l_2, l_3 + l_4)$, $l_1 + l_2 + L = \text{even}$, and $l_3 + l_4 + L = \text{even}$.

The groups (a) and (b) are most sensitive to non-Gaussian signals, as for which the unconnected terms (Eq.(6.3)) vanish on the full sky. On the other hand, the groups (c) and (d) are dominated by the unconnected terms, and thus less sensitive to non-Gaussianity. These statements should, however, depend upon what kind of non-Gaussianity exists in the data. If non-Gaussian signals are subject to the groups (c) and (d) only, then the groups (a) and (b) become the least sensitive modes to the non-Gaussianity.

On the incomplete sky, the unconnected terms also contaminate the groups (a) and (b) through the mode-mode coupling. We take this effect into account by using the Monte-Carlo simulations that use the same Galactic cut as the data.

We discriminate between the group (a) and the group (b) in terms of the covariance matrix: the covariance matrix of the group (a) is diagonal, while that of the group (b) is not diagonal in L. We discriminate between the group (c) and the group (d) in terms of the statistical power: the group (d) has no statistical power of testing Gaussianity. The reason is as follows. For the group (d), the estimator given by equation (6.2) becomes $T^{l_1 l_1}_{l_3 l_3}(0) = (-1)^{l_1+l_3}\sqrt{(2l_1+1)(2l_3+1)}C_{l_1}C_{l_3}$. The normalized bispectrum for the group (d) is thus just a pure number,

$$\frac{T^{l_1 l_1}_{l_3 l_3}(0)}{C_{l_1}C_{l_3}} = (-1)^{l_1+l_3}\sqrt{(2l_1+1)(2l_3+1)}. \tag{6.8}$$

This property holds regardless of Gaussianity. Even strongly non-Gaussian fields give exactly the same number. It thus follows from this result that we cannot measure the connected trispectrum for $L = 0$.

This is unfortunate. It is the connected part of $T^{l_1 l_1}_{l_3 l_3}(0)$ that contributes to the covariance matrix of the power spectrum,

$$\langle C_l C_{l'} \rangle - \langle C_l \rangle \langle C_{l'} \rangle = \frac{2 \langle C_l \rangle^2}{2l+1} \delta_{ll'} + \frac{(-1)^{l+l'}}{\sqrt{(2l+1)(2l'+1)}} \left\langle T^{ll}_{l'l'}(0) \right\rangle_{\rm c}, \tag{6.9}$$

where $\left\langle T^{ll}_{l'l'}(0) \right\rangle_{\rm c}$ is the ensemble average of the connected $T^{ll}_{l'l'}(0)$. Even if we find the groups (a)–(c) consistent with Gaussianity, we can conclude nothing about the power spectrum covariance, unless we have a model for the connected trispectrum. We will discuss this point in § 6.4.

Henceforth, we analyze the groups (a)–(c) only, while we have used the group (d) to see if our code works properly. Our code reproduces equation (6.8) very well, and the numerical error is at most of order 10^{-4}.

6.3.2 Gaussianity test

To quantify statistical significance of the measured trispectrum, we use a statistic P, which is the probability of the measured normalized trispectrum being greater than those drawn from the Monte–Carlo simulations:

$$P_\alpha \equiv \frac{N\left(\left|J_\alpha^{\rm DMR}\right| > \left|J_\alpha^{\rm MC}\right|\right)}{N_{\rm total}}, \tag{6.10}$$

where J_α denotes the normalized trispectrum, $N_{\rm total} = 30,000$ is the total number of the simulated realizations, and α represents a set of (l_1, l_2, l_3, l_4, L). The distribution of P_α is uniform if the DMR map is consistent with Gaussian, for which there are equal number of modes in each bin of P. For example, when we calculate P_α for all 21,012 α's, we expect a Gaussian field to give 210.12 modes in $\Delta P = 1\%$ bin. If we detect the normalized trispectrum significantly, then the number of modes having higher P is much larger than the expectation value for a Gaussian field.

In chapter 5, we have proven the P distribution uniform, if the DMR data are consistent with the simulated realizations (see Eq.(5.9)). We have also shown that this property holds regardless of the distribution function of $J_\alpha^{\rm MC}$.

We calculate the KS statistic for the P distribution in comparison with the uniform distribution, to quantify how well the P distribution is uniform. We calculate the KS statistic for the groups (a)–(c) separately. Table 6.1 summarizes the KS-test results, and figures 6.2–6.4 plot the cumulative P distribution, for which we have calculated the KS statistic. We find that the measured trispectrum is comfortably consistent with Gaussianity for all of the analyzed groups, (a)–(c).

Since the groups (a) and (b) are zero for Gaussian fields, these groups provide the strongest constraint on generic non-Gaussian fluctuations. As we have done in chapter 5 for the angular bispectrum, if we have predictions for the CMB angular trispectrum (e.g., appendix D), then our measurement tests those predictions.

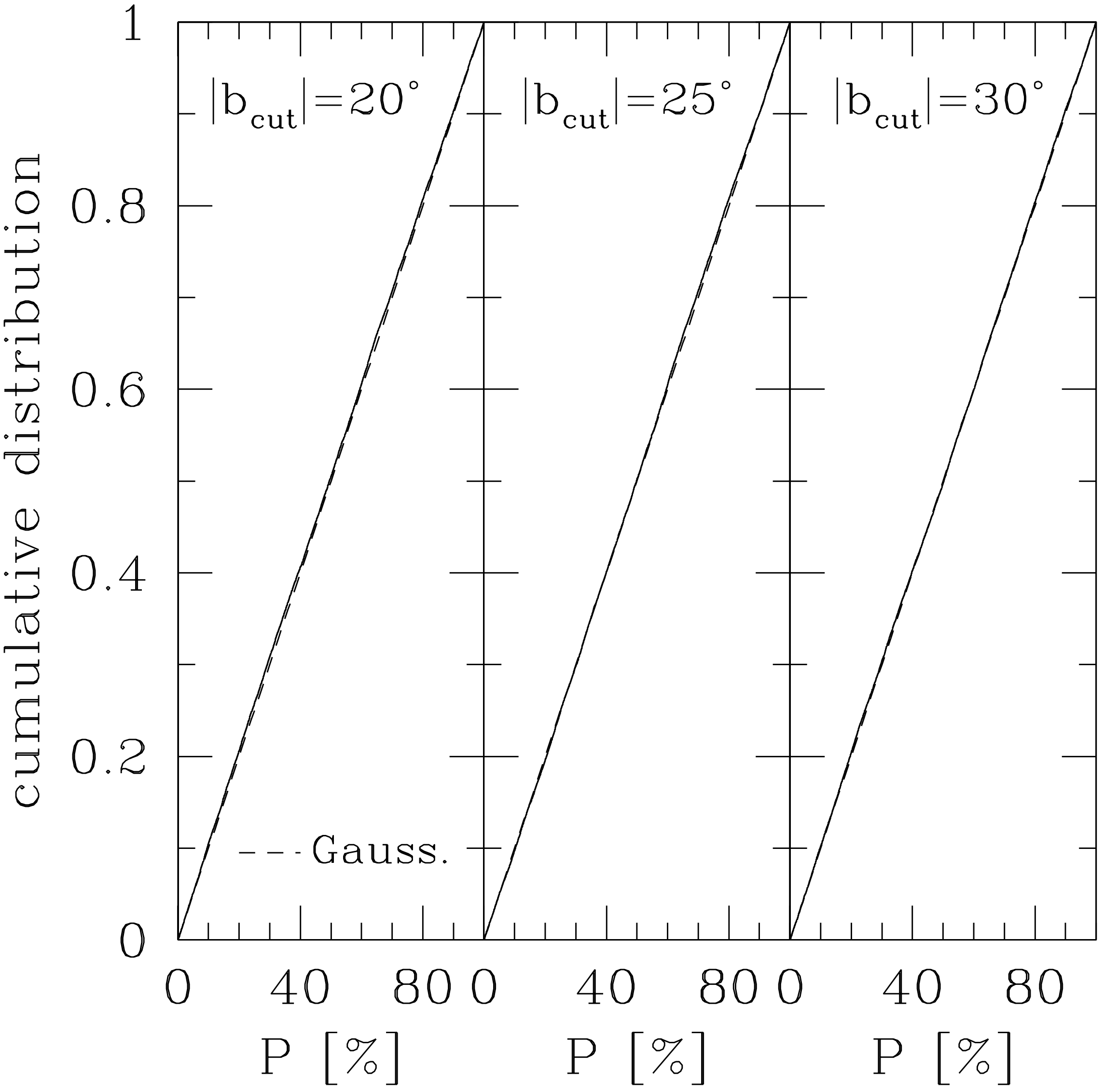

Figure 6.2: KS Test for Gaussianity with Trispectrum I

Cumulative P Distribution (Eq.(6.10)), for which we calculate the KS statistic. P is the probability of the normalized trispectrum, $T^{l_1 l_2}_{l_3 l_4}(L)/\left[(2L+1)C_{l_1}C_{l_2}C_{l_3}C_{l_4}\right]^{1/2}$, for the group (a) ($L \neq 0$ and $l_1 \leq l_2 < l_3 \leq l_4$), measured on the *COBE* DMR 53 + 90 GHz sky map, being larger than those drawn from the Monte–Carlo simulations. There are 16,654 modes. From left to right panels, we use the 20°, 25°, and 30° Galactic cuts, respectively. The dashed lines show the expectation value for a Gaussian field. The KS statistic gives the probability of the distribution being consistent with Gaussianity as 5.4%, 12%, and 48% for the three Galactic cuts, respectively.

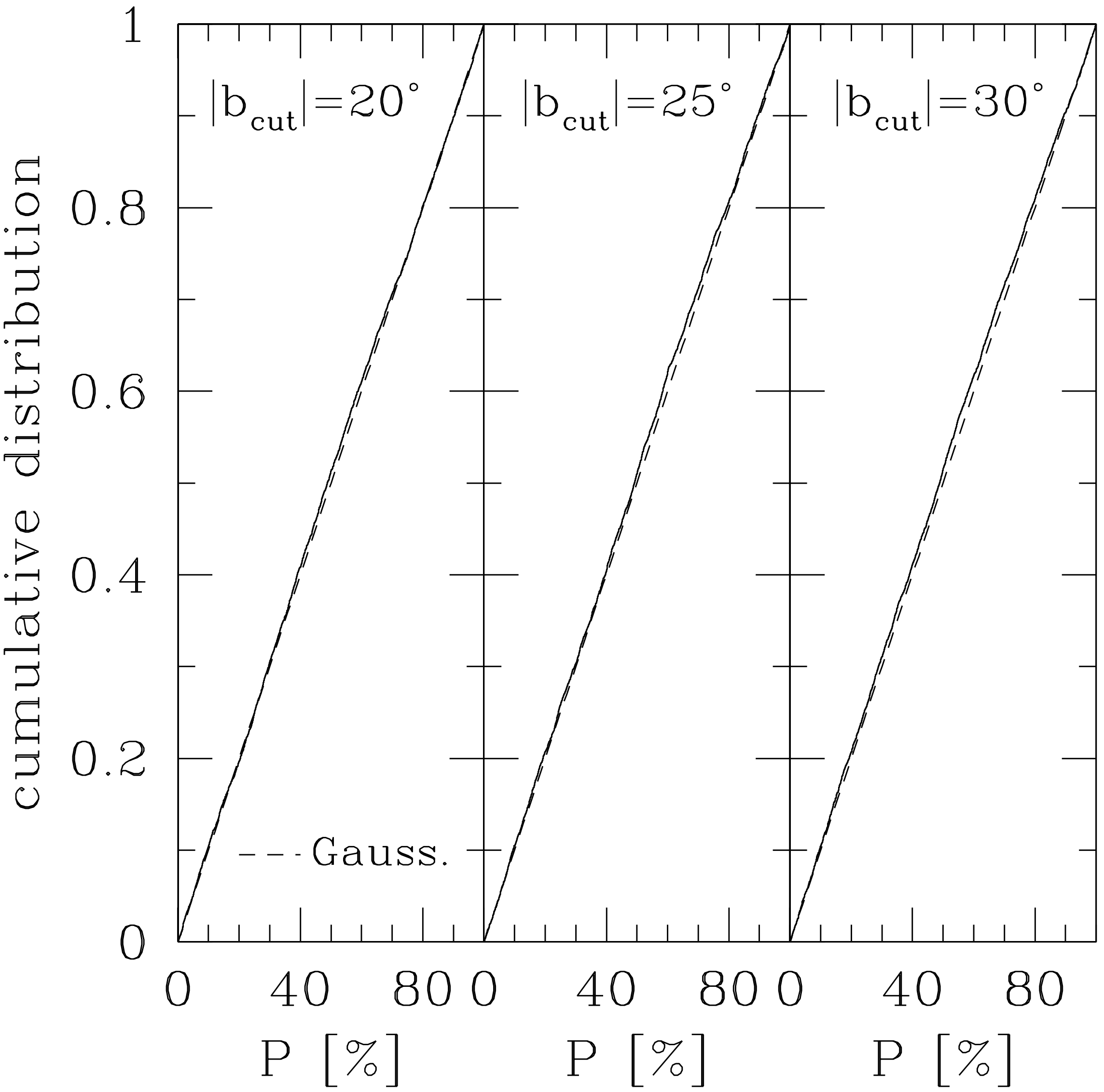

Figure 6.3: KS Test for Gaussianity with Trispectrum II

The same as figure 6.2 but for the group (b) ($l_2 = l_3$, $l_1 \neq l_4$, and $L \neq 0$). There are 4,059 modes. The KS statistic gives the probability of the distribution being consistent with Gaussianity as 38%, 2.5%, and 5.2% for the three Galactic cuts, respectively.

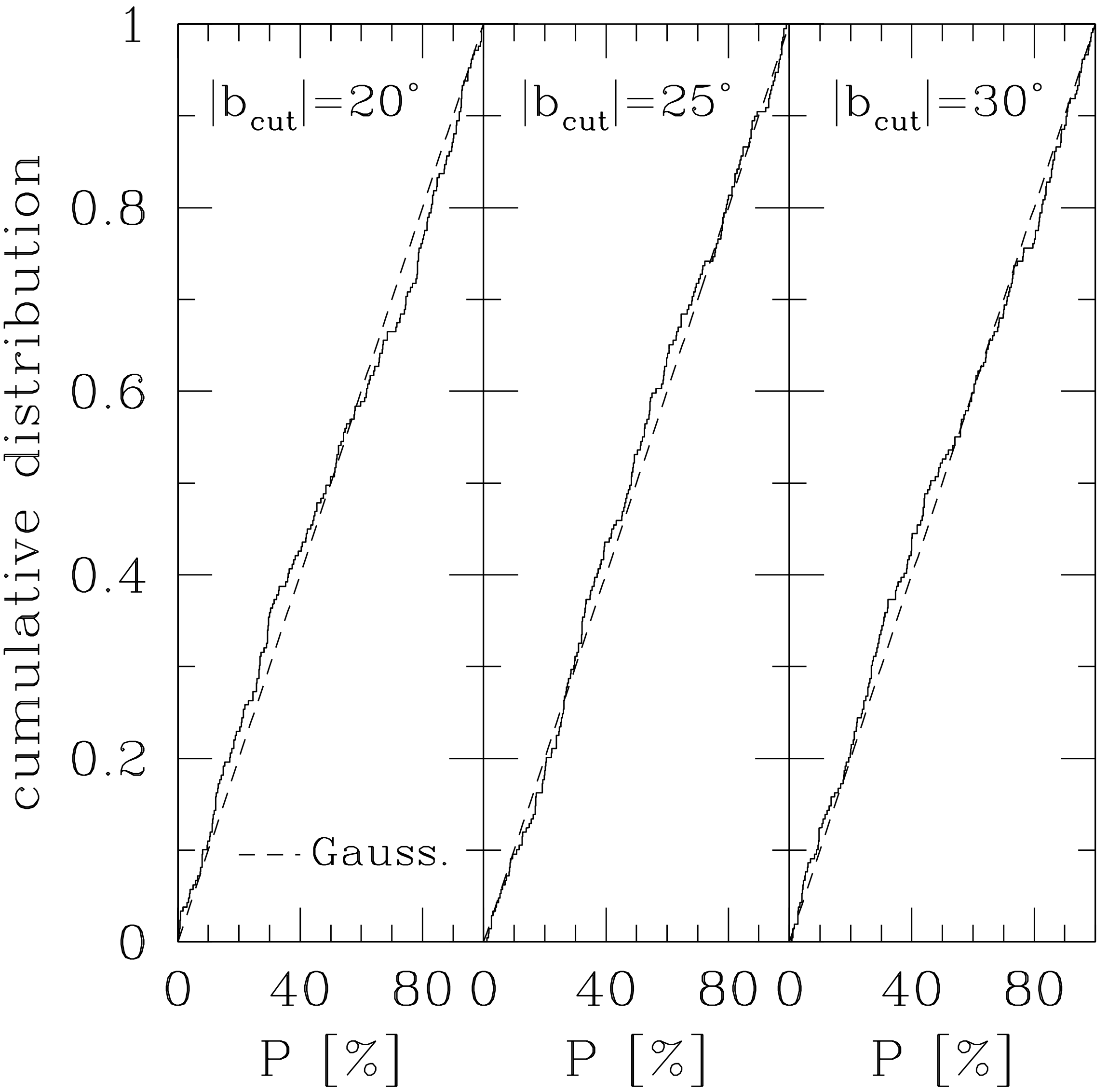

Figure 6.4: KS Test for Gaussianity with Trispectrum III

The same as figure 6.2 but for the group (c) ($l_1 = l_2 = l_3 = l_4$ and $L \neq 0$). There are 209 modes. The KS statistic gives the probability of the distribution being consistent with Gaussianity as 41%, 73%, and 63% for the three Galactic cuts, respectively.

Table 6.1: Gaussianity Test with Normalized Trispectrum

Probability of the measured trispectrum being consistent with Gaussianity (the rightmost column) for the three different Galactic cuts. The probability is derived from the KS test for the P distribution in comparison with the uniform distribution. The group (a) comprises the modes of $l_2 \neq l_3$, and $L \neq 0$ (16,554 modes), the group (b) of $l_2 = l_3$, $l_1 \neq l_4$, and $L \neq 0$ (4,059 modes), and the group (c) of $l_1 = l_2 = l_3 = l_4$, and $L \neq 0$ (209 modes).

group	# of modes	Galactic cut	probability [%]
(a)	16,554	20°	5.4
		25°	12
		30°	48
(b)	4,059	20°	38
		25°	2.5
		30°	5.2
(c)	209	20°	41
		25°	71
		30°	63

6.4 Discussion and Conclusions

In this chapter, we have presented the first measurement of the CMB angular trispectrum on the *COBE* DMR sky maps. We have measured all the trispectrum terms, 21,012 terms, down to the DMR beam size. Since 190 $L = 0$ modes have no statistical power of testing Gaussianity, we have used 20,822 $L \neq 0$ modes to test Gaussianity of the DMR data, and found that the DMR map is comfortably consistent with Gaussianity.

Our results do not directly constrain the connected trispectrum for $L = 0$, $T^{ll}_{l'l'}(0)$, which contributes to the power spectrum covariance through equation (6.9). We can thus conclude nothing as to whether the covariance matrix is diagonal on the DMR angular scales. Moreover, $T^{ll}_{ll}(0)$ increases the power spectrum variance; we have no idea how much the contribution is. We need to use other statistics than the angular trispectrum to investigate the power spectrum covariance. Otherwise, we have to have a model for the connected trispectrum, and constrain $T^{ll}_{l'l'}(0)$ by measuring the other trispectrum configurations.

One example for a trispectrum model is the one produced in a closed hyperbolic universe. Inoue (2001b) suggests that the closed hyperbolic geometry produces non-zero connected trispectrum. In appendix D, we have derived an analytic prediction for the connected trispectrum produced in a closed hyperbolic universe (Eq.(D.9)). For $L = 0$, we reduce the prediction to

$$\left\langle T^{l_1 l_1}_{l_3 l_3}(0) \right\rangle_{\mathrm{c}} = (-1)^{l_1+l_3} \sqrt{(2l_1+1)(2l_3+1)}\,(2F_{l_1 l_3}) + 4F_{l_1 l_1}\delta_{l_1 l_3}, \tag{6.11}$$

where

$$F_{l_1 l_3} = \sum_{\nu} P^2_{\Phi}(\nu) g^2_{\mathrm{T}l_1}(\nu) g^2_{\mathrm{T}l_3}(\nu) \left\langle |\xi_{l_1 m_1}(\nu)|^2 \right\rangle \left\langle |\xi_{l_3 m_3}(\nu)|^2 \right\rangle, \tag{6.12}$$

and $\nu = \sqrt{k^2 - 1}$ is a discrete wavenumber, $\Phi(\nu)$ is the primordial curvature perturbation, $g_{\mathrm{T}l}(\nu)$ is the radiation transfer function, and $\xi_{lm}(\nu)$ describes eigenmodes in a closed hyperbolic geometry. Hence, a single function, $F_{ll'}$, determines the connected trispectrum completely.

$F_{ll'}$ contributes to the power spectrum covariance directly. Using the prediction, we find the power spectrum covariance matrix in a closed hyperbolic universe (Eq.(D.10)),

$$\langle C_l C_{l'} \rangle - \langle C_l \rangle \langle C_{l'} \rangle = \frac{2}{2l+1} \left(\langle C_l \rangle^2 + 2F_{ll} \right) \delta_{ll'} + 2F_{ll'}. \tag{6.13}$$

The power spectrum is given by

$$\langle C_l \rangle = \sum_{\nu} P_{\Phi}(\nu) g_{\mathrm{T}l}^2(\nu) \left\langle |\xi_{lm}(\nu)|^2 \right\rangle. \tag{6.14}$$

Note that $\langle C_l \rangle \langle C_{l'} \rangle \geq F_{ll'}$. It follows from this equation that to constrain the contribution of the connected $T^{ll}_{l'l'}(0)$ to the power spectrum covariance, we need to constrain $F_{ll'}$.

In addition to $L = 0$ modes, fortunately, a closed hyperbolic universe also produces the connected trispectrum for the group (c), $l_1 = l_2 = l_3 = l_4 \equiv l$ and $L \neq 0$. The prediction is $\left\langle T^{ll}_{ll}(L) \right\rangle_{\mathrm{c}} = 4(2L+1)F_{ll}$. We may constrain this term with our measurement of the group (c). The group (c) is, however, the most noisy group, and the constraint from the DMR measurement is too weak to be useful yet.

The most promising way to investigate the angular trispectrum in near future is to use the *MAP* CMB sky maps. The big advantage of *MAP* over *COBE* is the much higher angular resolution. The high-resolution measurement is important even on large angular scales, as we can minimize the effect of the Galactic cut. Since the rather big *COBE* Galactic cut has been the main cause of numerous complications in the data analysis, we expect that the *MAP* data will measure the angular trispectrum with much better sensitivity, and with much smaller systematic errors than *COBE*. The *MAP* trispectrum will put strong constraints on several challenging non-Gaussian models: the non-Gaussianity induced from topology of the universe, the weak lensing effect, and so on, which are not probed by the angular bispectrum.